



Autophagy Regulation Influences β -Amyloid Toxicity in Transgenic *Caenorhabditis elegans*

Hongru Lin, Yehui Gao, Chen Zhang, Botian Ma, Mengchen Wu, Xianghuan Cui* and Hongbing Wang*

Putuo People's Hospital, School of Life Sciences and Technology, Tongji University, Shanghai, China

OPEN ACCESS

Edited by:

Ralf J. Braun,
Danube Private University, Austria

Reviewed by:

Per Evert Tore Nilsson,
Karolinska Institutet (KI), Sweden
Thomas Enzlein,
Mannheim University of Applied
Sciences, Germany
Suraiya Saleem,
Sathyabama Institute of Science
and Technology, India

*Correspondence:

Xianghuan Cui
cuixh@tongji.edu.cn
Hongbing Wang
hbwang@tongji.edu.cn

Specialty section:

This article was submitted to
Alzheimer's Disease and Related
Dementias,
a section of the journal
Frontiers in Aging Neuroscience

Received: 27 February 2022

Accepted: 13 April 2022

Published: 12 May 2022

Citation:

Lin H, Gao Y, Zhang C, Ma B,
Wu M, Cui X and Wang H (2022)
Autophagy Regulation Influences
 β -Amyloid Toxicity in Transgenic
Caenorhabditis elegans.
Front. Aging Neurosci. 14:885145.
doi: 10.3389/fnagi.2022.885145

Alzheimer's disease (AD) is a progressive, neurodegenerative disease characterized by the accumulation of amyloid-beta ($A\beta$) proteins in the form of plaques that cause a proteostasis imbalance in the brain. Several studies have identified autophagy deficits in both AD patients and AD animal models. Here, we used transgenic *Caenorhabditis elegans* to study the relationship between autophagy flux and $A\beta$. We labeled autophagosomes with an advanced fluorescence reporter system, and used this to observe that human $A\beta$ expression caused autophagosome accumulation in *C. elegans* muscle. The autophagy-related drugs chloroquine and 3-MA were employed to investigate the relationship between changes in autophagic flux and the toxicity of $A\beta$ expression. We found that reducing autophagosome accumulation delayed $A\beta$ -induced paralysis in the CL4176 strain of *C. elegans*, and alleviated $A\beta$ -induced toxicity, thus having a neuroprotective effect. Finally, we used RNA-sequencing and proteomics to identify genes whose expression was affected by $A\beta$ aggregation in *C. elegans*. We identified a series of enriched autophagy-related signal pathways, suggesting that autophagosome accumulation impairs $A\beta$ protein homeostasis in nematodes. Thus, maintaining normal autophagy levels appears to be important in repairing the protein homeostasis imbalance caused by $A\beta$ expression.

Keywords: *Caenorhabditis elegans*, autophagy, RNA-sequencing, quantitative proteomics, Alzheimer's disease

INTRODUCTION

Alzheimer's disease (AD) is a devastating neurodegenerative disorder with no known cure (Savelieff et al., 2019). Multiple factors, such as amyloid-beta ($A\beta$) peptide aggregation (Selkoe and Hardy, 2016), tau-protein hyperphosphorylation (Mangialasche et al., 2010), inflammatory processes (Martin et al., 2017), and oxidative stress (Huang and Mucke, 2012), are considered to be causative of AD. Additionally, growing evidence suggests that autophagy deficits promote the progression of AD (Li et al., 2017). The extensive accumulation of immature autophagosomal vesicles has been observed in the AD brain, suggesting that autophagic proteolysis may be seriously compromised in this disease (Florez-McClure et al., 2007). The phenomenon of autophagosome accumulation is also noted in the $A\beta$ transgenic *Caenorhabditis elegans* strain CL4176 (Florez-McClure et al., 2007).

Transgenic *C. elegans* expressing human $A\beta$ have been used as AD model systems because of their short lifespan, well-characterized genome, and considerable homology with human genomes (Sorrentino et al., 2017). Various AD nematode models have been developed to investigate the

molecular mechanism of A β toxicity and to screen therapeutic agents. These include GMC101, which expresses full-length A β _{1–42} in the body wall muscle (Sorrentino et al., 2017); CL4176, which is an effective model for screening AD drugs with potential therapeutic effects (Drake et al., 2003); and CL2355, which expresses A β in the neurons, and is used to observe A β -induced neuronal changes (Wu et al., 2006).

Based on the extremely complex pathogenesis of AD, the work of finding new therapeutic targets from pathology has become particularly important. We hope to explore the relationship between autophagy regulation and A β toxicity through transgenic nematode models. In the present study, we found that autophagy dysfunction caused an imbalance in protein homeostasis in A β transgenic strain GMC101. The intracellular expression of A β caused autophagosome accumulation, enhanced lysosomal activity, activated the rapamycin signaling pathway. Moreover, autophagy dysfunction resulted in oxidative stress and increased the accumulation of A β . While inhibiting the formation of autophagosomes delayed paralysis and had a neuroprotective effect. These results suggest the need to focus on the differential changes of autophagy during early stages of AD, and to maintain a stable autophagy flux while formulating AD treatment plans.

MATERIALS AND METHODS

Strains and Maintenance Conditions

Caenorhabditis elegans strains CL4176 [(pAF29) myo-3p:A β _{1–42} + (pRF4) rol-6 (su1006)]; CL2355 [pCL45 (snb-1:Abeta 1-42:3'-UTR (long) + mtl-2:GFP); GMC101 [unc-54p:A-beta-1-42:unc-54 3'-UTR + mtl-2p:GFP]; and CL2122 [(pPD30.38) unc-54 (vector) + (pCL26) mtl-2:GFP] were obtained from the *Caenorhabditis* Genetics Center (CGC; Minneapolis, MN, United States). If there is no special instructions, all strains are stored at 20°C. The worms were cultured on solid nematode growth medium (NGM) (Chen et al., 2020) plates containing a lawn of *Escherichia Coli* (*E. coli*) OP50.

The strains were routinely cultured and maintained at 16°C (for CL4176 and CL2355) on nematode growth medium (NGM) seeded with *Escherichia coli* OP50. From larval stage 1 (L1) or the young adult stage, they were fed with small molecule drugs 3-methyladenine (3-MA) (S2767, Selleck, China) or chloroquine (CQ) (S6999, Selleck, China) to interfere with autophagy flux. 3-MA is a selective phosphoinositide 3-kinase (PI3K) inhibitor that blocks autophagy through its action on phosphoinositide 3-phosphate kinase, and PI3K activity is necessary for the nucleation and assembly of membrane pools in the early stages of autophagosome formation (Zeng and Zhou, 2008). And 3-MA could provide neuroprotective effects in cerebral ischemia injury models. Chloroquine is a lysosomotropic weak base, which in the monoprotonated form diffuses into the lysosome, where it becomes diprotonated and becomes trapped. Protonated chloroquine then changes the lysosomal pH, thereby inhibiting autophagic degradation in the lysosomes. It is generally believed that CQ could deacidify lysosomes and inhibit autophagy (Palmisano et al., 2017).

Construction of Transgenic Strains

Plasmid *lgg-1p:mCherry:GFP:lgg-1* (pMH878) was a gift from Professor Malene Hansen (Chang et al., 2017). Transgenic GMC101 or CL2122 strains expressing an extrachromosomal array were created by the gonadal microinjection of pMH878 (100 μ g/ml) (Chang et al., 2017), which was subsequently integrated by γ -irradiation followed by outcrossing four times to GMC101 or CL2122 strains (Chang et al., 2017).

RNA Sequencing (RNA-Seq)

GMC101 and CL2122 strains were synchronized (Fabian and Johnson, 1994), and their eggs allowed to hatch and develop to the young adult stage on NGM plates at 20°C. Then, the temperature was increased to 25°C to induce A β expression for 8 or 24 h. Gene expression in GMC101 and CL2122 strains was assessed by Novo Gene Corporation (Beijing, China). Sequencing libraries were generated using NEBNext[®] Ultra[™] RNA Library Prep Kit for Illumina[®] (NEB, United States) following manufacturer's recommendations and index codes were added to attribute sequences to each sample. In order to select cDNA fragments of preferentially 250~300 bp in length, the library fragments were purified with AMPure XP system (Beckman Coulter, Beverly, United States). Then 3 μ l USER Enzyme (NEB, United States) was used with size-selected, adaptor-ligated cDNA at 37°C for 15 min followed by 5 min at 95°C before PCR. Then PCR was performed with Phusion High-Fidelity DNA polymerase, Universal PCR primers and Index (X) Primer. At last, PCR products were purified (AMPure XP system) and library quality was assessed on the Agilent Bioanalyzer 2100 system. The clustering of the index-coded samples was performed on a cBot Cluster Generation System using TruSeq PE Cluster Kit v3-cBot-HS (Illumina) according to the manufacturer's instructions. After cluster generation, the library preparations were sequenced on an Illumina NovaSeq platform and 150 bp paired-end reads were generated. Up- or down-regulated genes were identified by filtering RNA-seq data with the following cut-off: a twofold change in expression level and a false discovery rate analog of $p < 0.05$. KEGG pathway enrichment was applied using "clusterProfiler" with criteria $p < 0.05$ (Yu et al., 2012). All raw data and detailed experimental methods have been uploaded to GEO database, GEO number: GSE198684. Information on differential genes is in **Supplementary Material**.

Quantitative Proteomics

GMC101 and CL2122 strains were synchronized, and their eggs allowed to hatch and develop to the young adult stage on NGM plates at 20°C. Then, the temperature was increased to 25°C to induce A β expression for 24 h. The label-free detection of protein expression in GMC101 and CL2122 strains was assessed by Novo Gene Corporation. A brief description is as follows: Peptides were separated in a home-made analytical column (15 cm \times 150 μ m, 1.9 μ m), using a linear gradient elution. The separated peptides were analyzed by Q Exactive[™] HF-X mass spectrometer (Thermo Fisher), with ion source of Nanospray Flex[™] (ESI), spray voltage of 2.1 kV and ion transport capillary temperature of 320°C. Full scan range from m/z 350 to 1,500

with resolution of 60,000 (at m/z 200), an automatic gain control (AGC) target value was 3×10^6 and a maximum ion injection time was 20 ms. The all resulting spectra were searched against database by the search engines: Proteome Discoverer 2.2 (PD 2.2, Thermo). Up- or down-regulated proteins were identified by filtering the data with the following cut-off: a twofold change in expression level and a false discovery rate analog of $p < 0.05$. Information on differential proteins is in **Supplementary Material**.

Quantification of Autophagic Vesicles

Caenorhabditis elegans were mounted live on a 2% agarose pad in M9 medium containing 0.1% NaN₃, and imaged using the Echo Revolve microscope at 40 \times . We selected the area above the pharynx of nematodes for statistics. The count method of mCherry::GFP::lgg-1-positive punctae was derived from the reported literature (Keith et al., 2016). Data were analyzed using one-way analysis of variance (ANOVA) or two-way ANOVA as applicable.

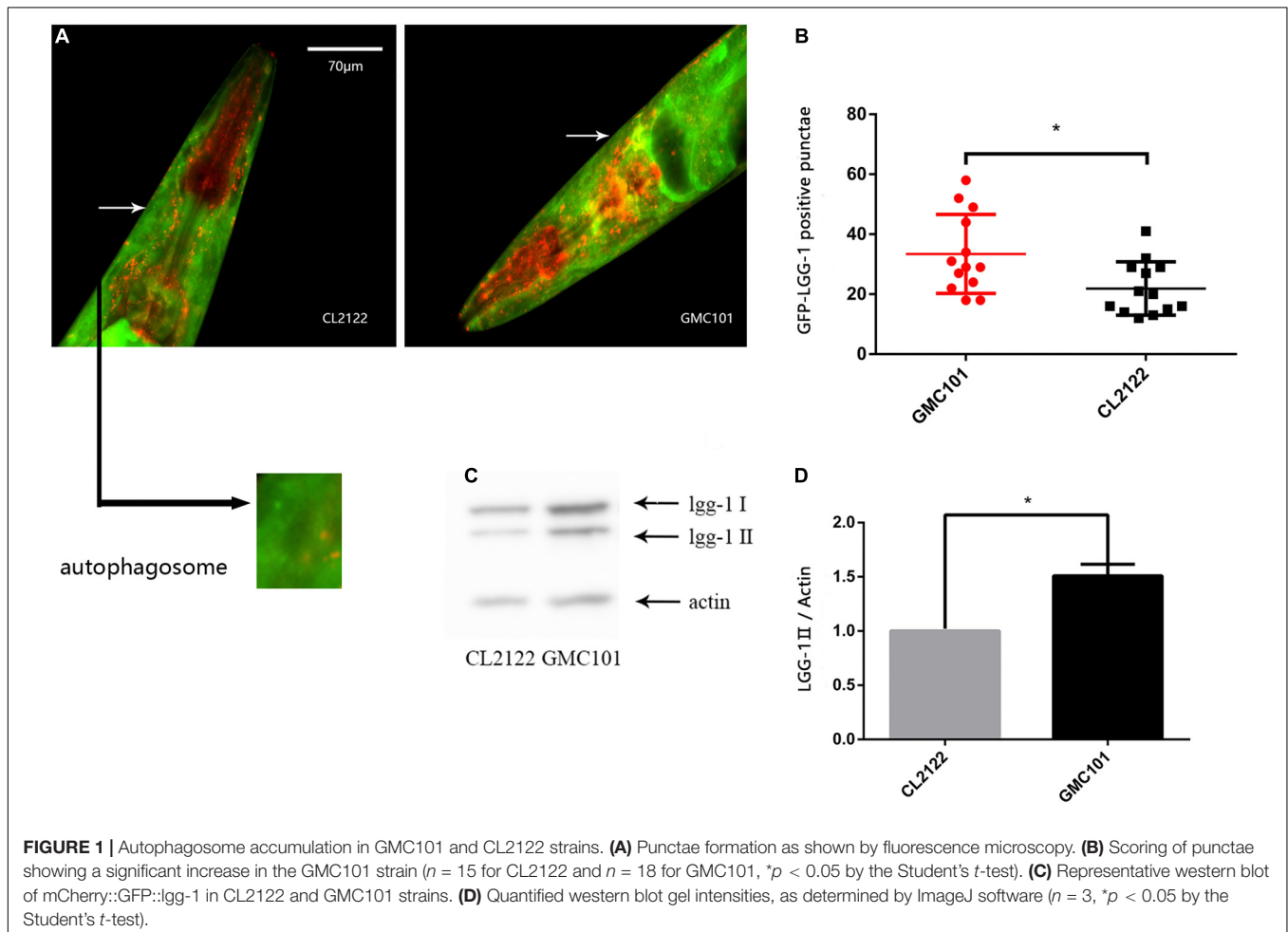
Paralysis Assay

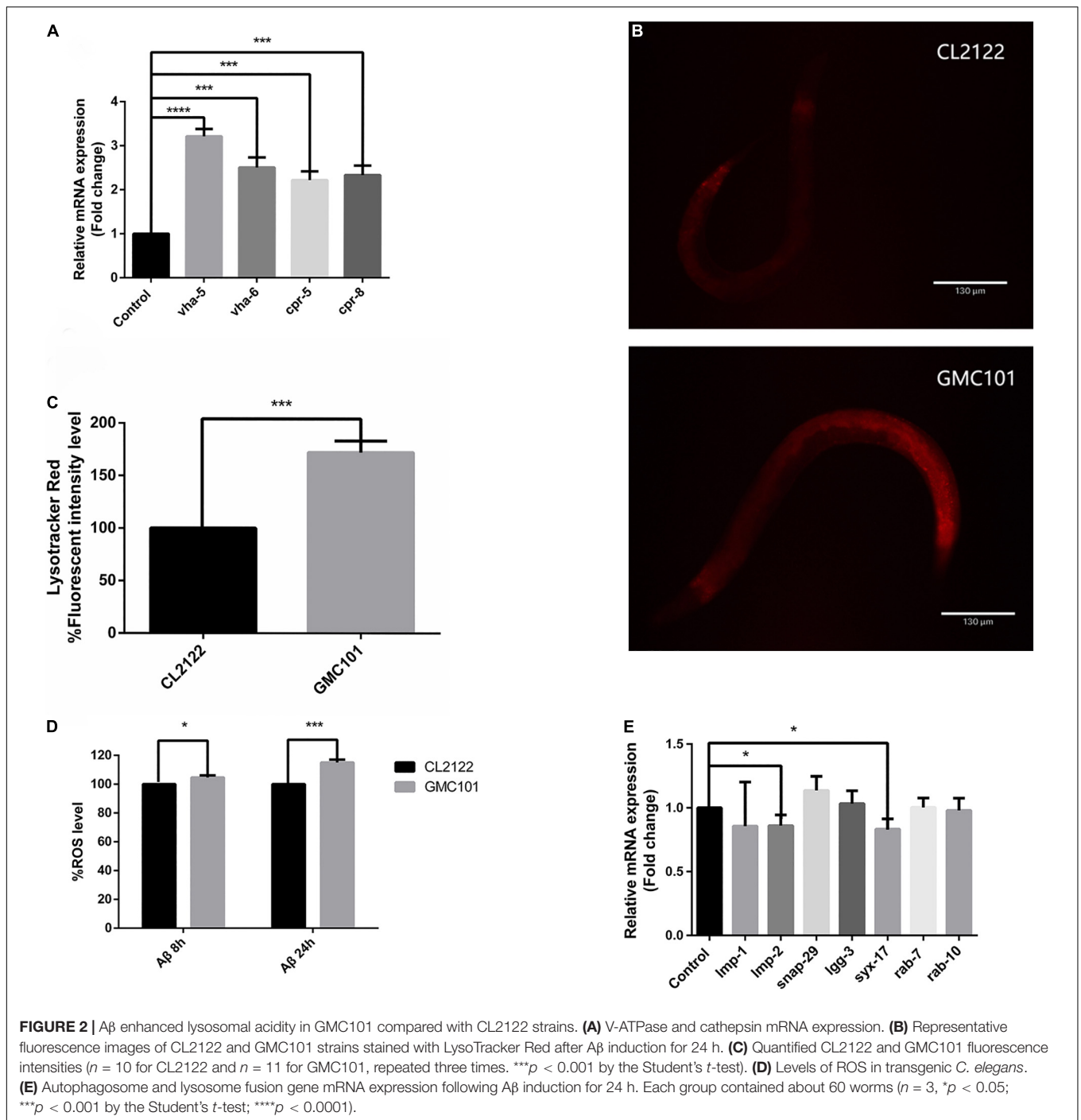
A β transgenic CL4176 nematodes were maintained on NGM at 16°C and synchronized (Zhang et al., 2016). They were treated

with or without drugs at stage L1 for 36 h, then transferred to 23°C for transgene induction. This temperature shift stimulated A β expression, causing A β aggregation and leading to paralysis. Scoring was begun 27 h after the temperature shift, and the nematodes were considered to be paralyzed if they failed to move their bodies when touched and produced a “halo” of cleared bacterial lawn because they only moved their heads while feeding. We used PT₅₀ as an index (the time interval from the onset of paralysis at which 50% of the nematodes were paralyzed). For example, a PT₅₀ of 4.1 h for the control was obtained by subtracting the onset time of paralysis, 29 h, from the time when 50% of the nematodes were paralyzed (33.1 h). The assay was performed at least three times. And each individual group contained more than 30 nematodes. Statistical analysis was conducted with GraphPad Prism 6.0 software, and p values were calculated using the log-rank test.

LysoTracker Red Staining

The acidophilic dye LysoTracker Red (C1046; Beyotime Biotechnology, Shanghai, China) (Imanikia et al., 2019) was used at a final concentration of 15 μ M. Synchronized GMC101 or CL2122 strains maintained at 20°C were treated with LysoTracker at stage L1 until the young adult stage,





then transferred to 25°C for transgene induction. After 24 h, nematodes were washed twice in fresh M9 (without LysoTracker) and imaged using a Revolve microscope (Imanikia et al., 2019).

Gene Expression Analysis by Quantitative PCR

Total RNA was extracted using Trizol A + (Tiangen, Beijing, China) and reverse-transcribed into cDNA. Expressed genes were amplified in triplicate and quantified by PCR using a SYBR Green

PCR Mix (B21702, Bimake, China) with the Roche LightCycler system. Data was analyzed using the $2^{-\Delta\Delta CT}$ method. The primer sequences used for quantitative PCR (qPCR) are provided in **Supplementary Material 1**.

RNA Interference

RNA interference (RNAi) experiments were based on a reported protocol (Li et al., 2018). In brief, RNA was delivered to nematodes by feeding, so gravid CL4176 adults were bleached,

and eggs were placed on NGM dishes containing 1 mM isopropyl β -D-1-thiogalactopyranoside (IPTG). An HT-115 (DE3) bacterial colony containing L4440 or the target gene plasmid was inoculated in LB broth containing 100 μ g/mL ampicillin and 12.5 μ g/mL tetracyclines, and grown for 8 h in a 37°C shaker. The bacteria were plated on the NGM dish containing IPTG 1 h prior to the addition of nematodes. The synchronized CL4176 strain was grown on RNAi NGM plates from eggs to adults for two generations. Synchronized L1 worms were treated with or without 3-MA or CQ for the paralysis assay as described above (Zhang et al., 2016).

Measurement of Reactive Oxygen Species

Endogenous reactive oxygen species (ROS) levels were measured using 2',7'-dichlorofluorescein diacetate (H2DCF-DA), which reacts with endogenous ROS to generate a fluorescent product (Yang et al., 2018). Nematodes were treated as in the paralysis assay, and ROS was measured at the point of paralysis. They were then incubated with 50 μ M H2DCF-DA for 30 min at 37°C, and the fluorescence intensity was measured at excitation and emission wavelengths of 485 and 535 nm, respectively. The assay was performed in triplicate.

Western Blotting

The GMC101 strain was synchronized, and eggs were allowed to hatch and develop to the L4 stage on NGM plates with or without 3-MA or CQ at 20°C. Then, the temperature was increased to 25°C and maintained for 24 h. Nematodes were collected from the plates with M9 buffer and washed twice to eliminate bacteria. Samples were heated at 100°C in sample loading buffer for 10 min and centrifuged at 10,000 g for 10 min (Sangha et al., 2015). Collected supernatant was boiled with loading buffer at 100°C for 5 min before being loaded into the gel. A 10–180 kDa protein marker (PR1910, Solarbio, China) was used as an indicator of molecular weight (Zhu et al., 2019). Samples were run at 40 V for 40 min on a stacking gel, and at 80 V for 120 min on a separating gel. The gel was then transferred to a

polyvinylidene fluoride membrane using 20% methanol transfer buffer at 100 V for 1 h. Blots were blocked in Tris-buffered saline with Tween 20 + 5% skimmed milk for 1 h. The A β protein levels were detected with 6E10 monoclonal antibody (dilution 1:500; 803014, BioLegend), with an anti- β -actin antibody (dilution 1:2,000; 60008, Proteintech) as a control. mCherry-GFP-LGG-1 was detected with a primary antibody against LGG-1 (dilution 1:1,000; Cell Signaling Technology). The horseradish peroxidase-conjugated goat anti-mouse antibody (1:2,000, Cell Signaling Technology) was used as the secondary antibody. Incubate the primary antibody overnight, and incubate the secondary antibody for 2 h at room temperature. Images were captured using a Chemscope 3400 mini western blot imaging system (Amersham Imager 600, GE, United States). Mean densities of the A β bands were analyzed using Image J software.

Chemotaxis Assays

The chemotaxis response in *C. elegans* is mediated by the activation of several sensory neurons and interneurons to stimulate motor neurons. Chemotaxis assays were performed as described previously (Wu et al., 2006). Synchronized transgenic *C. elegans* CL2355 and its control strain CL2122 were treated with or without 3-MA or CQ starting from L1 stage. They were cultured at 16°C for 36 h, then at 23°C for another 36 h, then collected and assayed in 100 mm plates. A total of 1 μ l 0.25 M sodium azide and 1 μ l odorant (0.5 M sodium acetate in 100% ethanol) were added to the “attractant” spot. On the opposite side of the attractant spot, 1 μ l control odorant (100% ethanol) and 1 μ l sodium azide were added. Immediately afterward, 2 μ l nematodes (n = approximately 60) were pipetted into the center of the plate, incubated at 23°C for 1 h, and the number of nematodes in each quadrant was scored. The chemotaxis index (CI) is a measure of the fraction of worms that move to the location of the attractant, and was calculated as follows:

$$CI = \frac{(\text{number of worms in both attractant quadrants} - \text{number of worms in both control quadrants})}{\text{total number of scored worms.}}$$

5-Hydroxytryptamine Sensitivity Assay

CL2355 worms were egg-synchronized and placed onto fresh NGM plates seeded with OP50, treated with or without 3-MA or CQ at 16°C for 36 h, then transferred to 23°C for 36 h. They were collected with M9 buffer, and the number of paralyzed worms after exposure to 5 mg/mL 5-hydroxytryptamine (5-HT) in a 96-well plate for 24 h was counted (Wu et al., 2006). The assay was performed at least three times.

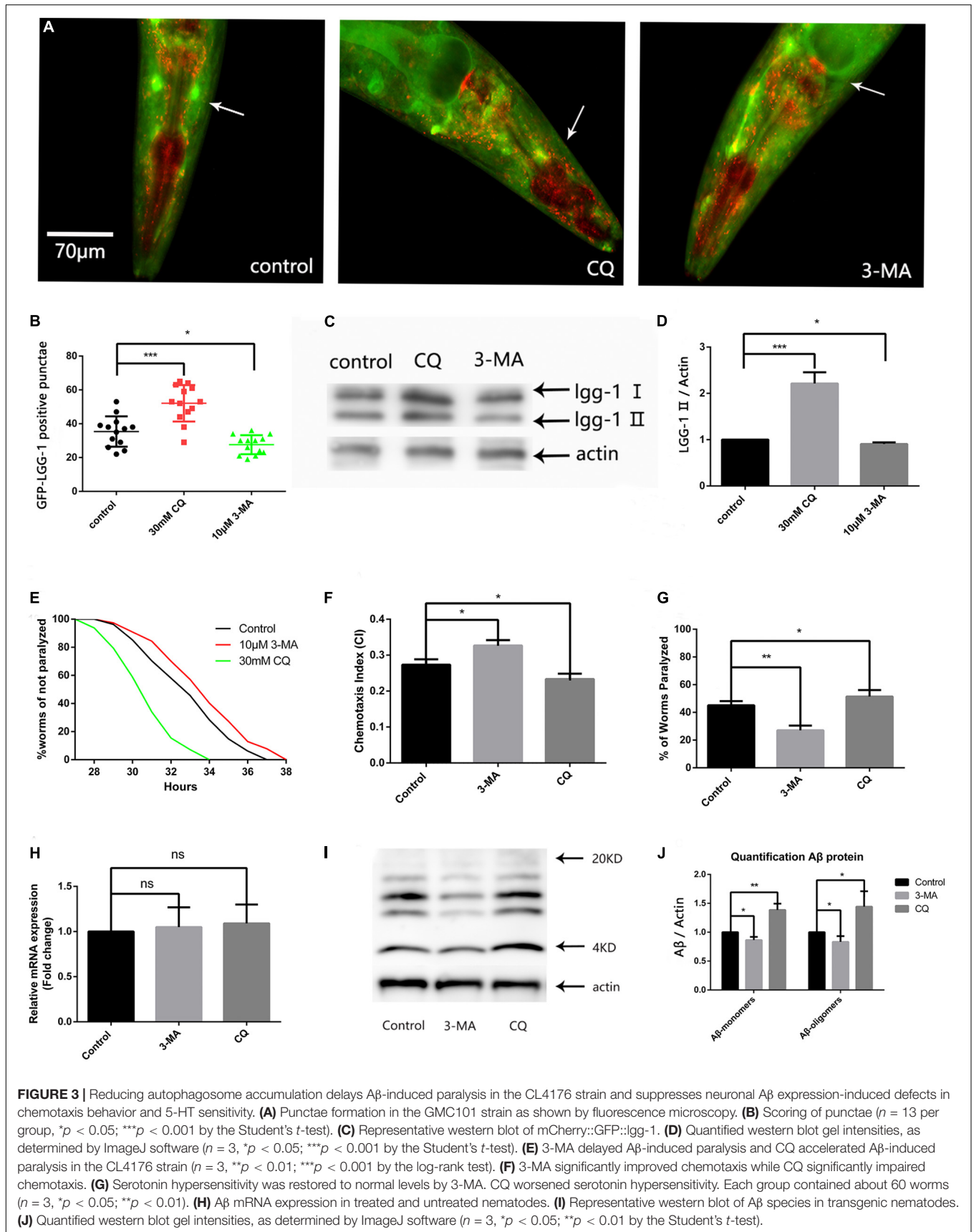
Statistical Analysis

GraphPad Prism 6.0 software was used for statistical analyses. For paralysis assays, p -values were calculated using the log-rank test. The Student's t -test was used to compare two groups. One-way ANOVA with Duncan's test was performed to compare multiple groups. $p < 0.05$ was considered statistically significant.

TABLE 1 | Differential gene expression verified by qPCR.

Gene ID	Fold Change (RNA-seq)	Fold Change (qPCR) \pm SEM
vha-5	3.5933	3.210 \pm 0.0981
vha-6	2.0691	2.507 \pm 0.1317
cpr-5	2.4064	2.217 \pm 0.1172
cpr-8	2.3219	2.333 \pm 0.1241
atg-16.2	0.3769	0.776 \pm 0.0058
epg-8	0.4476	0.672 \pm 0.0203
lgg-1	0.4691	0.663 \pm 0.0412
atg-4.2	0.3542	0.879 \pm 0.0057
atg-18	0.4426	0.732 \pm 0.0225
hsp-16.2	33.1284	8.002 \pm 1.710
hsp-70	15.6707	8.716 \pm 0.755

The experimental method and the number of repetitions have been stated in the method. The primer sequence is in **Supplementary Material 1**.



RESULTS

Human A β Expression Results in Autophagosome Accumulation in *Caenorhabditis elegans* Muscle

The accumulation of autophagic vacuoles at various stages of maturation has been reported in the CL4176 strain (Florez-McClure et al., 2007). In order to further confirm the phenomenon is widespread in transgenic A β strain, we constructed a dual-fluorescent mCherry:GFP:LGG-1 protein system using the GMC101(A β _{1–42}) strain and CL2122(control) strain to monitor autophagosomes by microinjection (Chang et al., 2017). With this reporter, autophagosomes are visualized as both GFP- and mCherry-positive punctae. By counting the number of GFP-LGG-1 positive punctae, we observed clear autophagosome accumulation in the GMC101 strain compared with the CL2122 strain (Figures 1A,B). To further confirm this, we used western blotting to measure the expression of lgg-1-II, which binds to autophagosomes (Springhorn and Hoppe, 2019). The protein level was significantly increased in the GMC101 strain compared with the CL2122 strain (Figures 1C,D), which was supportive of autophagosome accumulation in the A β transgenic strain.

Autophagosome Accumulation in GMC101 Is Not Due to Down-Regulated Lysosomal Acidity but Due to Reactive Oxygen Species-Mediated Abnormal Autophagosome Fusion

Decreased lysosomal acidity caused by aging has been identified as causative of abnormal autophagic flux in the brain of AD patients (Zare-Shahabadi et al., 2015). We speculated that autophagosome accumulation in the GMC101 strain is also associated with decreased lysosome acidity. To investigate this, we first measured mRNA expression levels of V-ATPase and cathepsin genes, which maintain lysosomal acidity (Ernstrom et al., 2012) and degrade A β (Hook et al., 2020), respectively. However, contrary to our expectations, the transcription of V-ATPase and cathepsin genes was significantly increased 24 h A β post-induction (Figure 2A and Table 1). To better observe A β -induced changes in lysosomal acidity, we carried out LysoTracker Red staining, and detected significantly increased levels of staining in the GMC101 strain compared with the CL2122 strain (Figures 2B,C). These results indicate that lysosomal acidity is enhanced in the GMC101 strain, suggesting its autophagosome accumulation is not caused by decreased lysosome acidity. In fact, A β induction appears to not only enhance the expression of lysosome-related genes but also to increase lysosomal acidity.

It was reported that A β induction could increase ROS levels in the transgenic APP mouse model (3 \times Tg-AD) (Ghosh et al., 2012), while ROS was shown to cause autophagosome accumulation (Wang et al., 2019). We evaluated the nematode redox status by measuring intracellular ROS levels with H₂DCF-DA (Figure 2D). The transcription

levels of autophagosome-lysosomal fusion genes were also measured (Figure 2E). Following A β induction, ROS levels increased while fusion-related gene transcription was down-regulated. This suggests that ROS prevented the fusion of autophagosomes and lysosomes.

Reducing Autophagosome Accumulation Delays A β -Induced Paralysis and Suppresses Neuronal A β Expression-Induced Defects in Chemotaxis Behavior and 5-Hydroxytryptamine Sensitivity

Because abnormally high ROS levels caused autophagosome accumulation (Wang et al., 2019), and abnormal organelles destroyed protein homeostasis, we next explored the effect of autophagosome accumulation on protein homeostasis. First, we used the fluorescent nematode mentioned in the above article to evaluate the effect of 3-MA and CQ on the number of GFP-LGG-1 positive punctae. Both fluorescence analysis (Figures 3A,B) and western blotting (Figures 3C,D) showed that 3-MA significantly reduced, while CQ aggravated, autophagosome accumulation.

Then we used the CL4176 model to evaluate the effect of autophagy intervention on protein homeostasis. Our results showed that 10 μ M 3-MA caused a delay in A β -induced paralysis, and that the PT₅₀ value was increased by 30.54% compared with the control (Figure 3E and Table 2). This suggests that inhibiting the formation and reducing the accumulation of autophagosomes has a protective effect against AD in nematodes. Conversely, 30 mM CQ significantly accelerated A β -induced paralysis and decreased the PT₅₀ value by 37.84% (Figure 3E and Table 2), showing the clear impact of lysosome deacidification on protein homeostasis. These results are consistent with the observed decrease in lysosomal activity mediated by aging responsible for autophagy dysfunction (Lipinski et al., 2010), which promotes the progression of AD.

Because limiting autophagosome accumulation delayed paralysis in the CL4176 strain, we next explored whether reducing autophagy accumulation had neuroprotective effects by characterizing the neuronal controlled behaviors of chemotaxis and 5-HT sensitivity in the CL2355 strain, in which A β is expressed in neuronal cells (Wu et al., 2006). The CI is a measure of the fraction of worms that are able to arrive at the location of the attractants. 5-HT is a key neurotransmitter that modulates several behaviors of *C. elegans*. When exogenous 5-HT is applied to the nematodes, they become paralyzed as a result of the sensitivity to excessive 5-HT (Wu et al., 2006).

Figure 3F shows that 10 μ M 3-MA significantly improved the CI compared with the untreated control (CI_{control}, 0.2733 \pm 0.0088 vs. CI_{3-MA}, 0.3300 \pm 0.0057, $n = 3$, ** $p < 0.01$), suggesting that 3-MA has a significant neuroprotective effect in nematodes. We also found that 30 mM CQ significantly reduced the CI compared with the control (CI_{control}, 0.2733 \pm 0.0088 vs. CI_{CQ}, 0.2333 \pm 0.0088, $n = 3$, * $p < 0.05$).

Using the ability of nematodes to take up exogenous 5-HT, we next evaluated the effects of 3-MA and CQ on the nematode

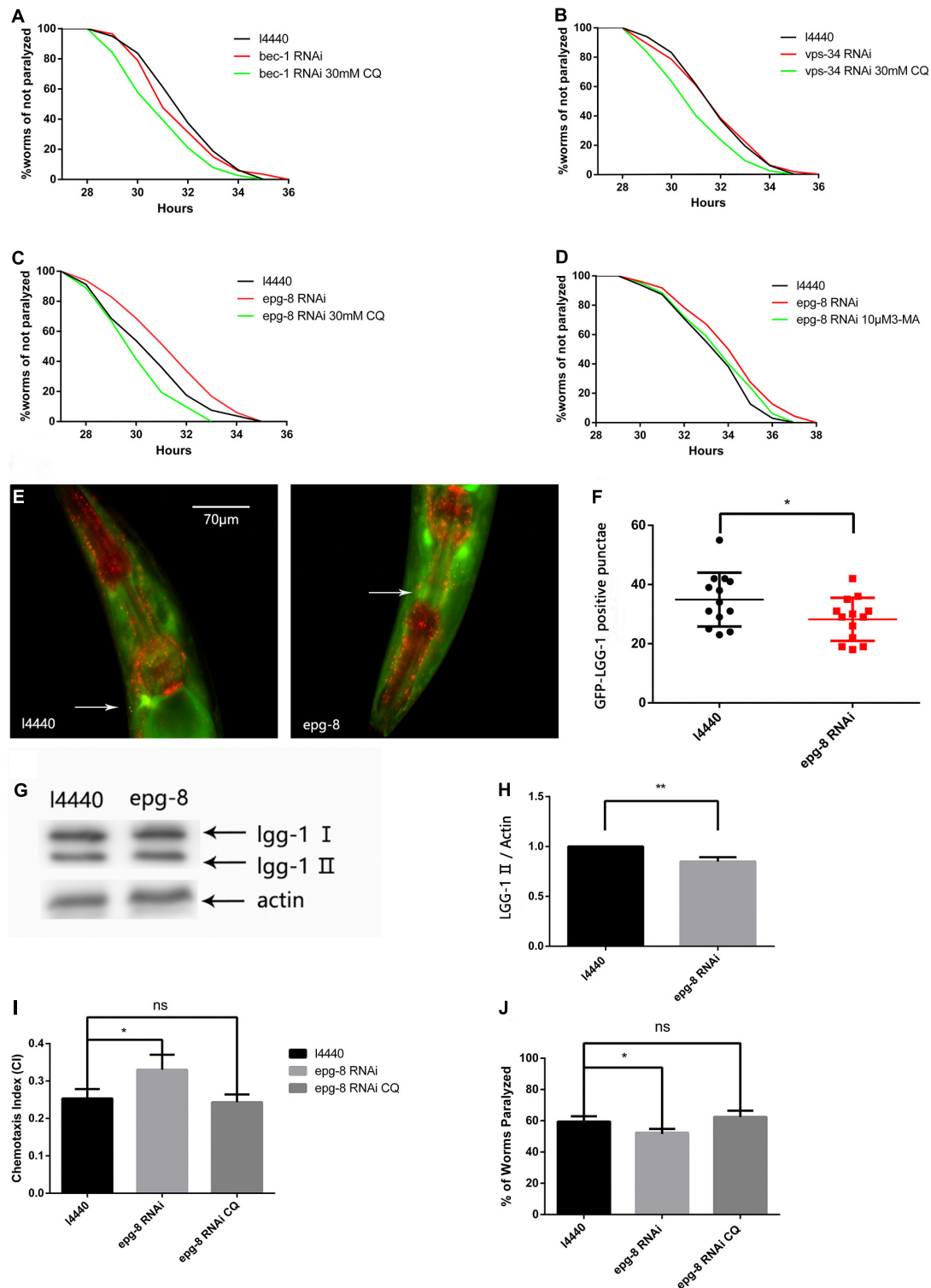


FIGURE 4 | The CL4176 strain was fed either vector I4440 control bacteria or bacteria expressing RNAi for *bec-1* (A), *vps-34* (B), or *epg-8* (C,D). RNAi of *epg-8* delayed A β -induced paralysis which could be offset by CQ. ($n = 3$, * $p < 0.05$ by the log-rank test). Each individual group contains more than 30 nematodes. (E) Punctae formation in the GMC101 strain with or without RNAi bacteria as shown by fluorescence microscopy. (F) Scoring of punctae with or without RNAi bacteria ($n = 13$ per group, * $p < 0.05$ by the Student's t -test). (G) Representative western blot of mCherry::GFP::lgg-1. (H) Quantified western blot gel intensities, as determined by ImageJ software ($n = 3$, ** $p < 0.01$ by the Student's t -test). (I) Chemotaxis of the CL2355 strain fed either vector I4440 control bacteria or bacteria expressing RNAi for *epg-8*. (J) Serotonin hypersensitivity was restored by *epg-8* RNAi and reversed by CQ. Each group contains about 60 worms ($n = 3$, * $p < 0.05$).

nervous system. **Figure 3G** shows a percentage paralysis of 3-MA-treated worms of $27.00 \pm 1.98\%$ and CQ-treated worms of $53.23 \pm 1.19\%$, compared with the control of $45.10 \pm 1.75\%$. Therefore, $10 \mu\text{M}$ 3-MA ameliorated the phenotypic defect in the CL2355 strain, while it was made worse by 30 mM CQ. Thus, the inhibition of autophagosome formation by 3-MA exerted a significant neuroprotective effect in the nematode model of A β -induced neurotoxicity, while abnormal autophagosome degradation exacerbated A β -induced neurotoxicity.

To further evaluate protein homeostasis in nematodes, we measured the level of A β mRNA by qPCR, but found no significant difference between 3-MA-treated and CQ-treated nematodes (**Figure 3H**). However, western blotting of A β protein levels (Sangha et al., 2015) showed that 30 mM CQ significantly increased the expression of A β monomers (fold-change: 1.387 ± 0.062 , $n = 3$, $**p < 0.01$) and oligomers (fold-change: 1.443 ± 0.153 , $n = 3$, $*p < 0.05$) (**Figure 3I**). Moreover, $10 \mu\text{M}$ 3-MA significantly reduced the expression of A β monomers (fold-change: 0.863 ± 0.031 , $n = 3$, $*p < 0.05$) and oligomers (fold-change: 0.833 ± 0.057 , $n = 3$, $*p < 0.05$) (**Figure 3J**). This phenomenon may be associated with the alleviation of autophagosome accumulation, and requires further exploration.

Autophagosome Reduction by the PI3K Complex Delays A β -Induced Paralysis in CL4176 Nematodes and Has a Neuroprotective Effect

Because the PI3K inhibitor 3-MA delayed paralysis, we next determined whether suppressing PI3K gene transcription would have the same effect. We used RNAi to decrease the expression of PI3K complex-related genes (**Figures 4A–C**) *bec-1*, *vps-34*, and *epg-8* (Zhang and Baehrecke, 2015). **Figure 4C** shows that *epg-8* RNAi delayed A β -induced paralysis, and increased the PT₅₀ value by 26.01% compared with the control (**Table 2**). While *bec-1* or *vps-34* RNAi did not prolong paralysis. Then we performed RNAi on the fluorescent model. Autophagosome

accumulation was significantly reduced (**Figures 4E–H**) when we reduced the expression of *epg-8* by RNAi, indicating that reducing autophagosome accumulation alleviates A β -induced toxicity. No significant differences were observed after intervention on the other two genes. CI and 5-HT sensitivity results also provided strong support for this (**Figures 4I, J**), with *epg-8* RNAi significantly increasing the CI compared with the control (CI_{14440} , 0.2533 ± 0.0145 vs. $CI_{epg-8\text{RNAi}}$, 0.3300 ± 0.0231 , $n = 3$, $*p < 0.05$). Moreover, *epg-8* RNAi worms had a percentage paralysis of $59.43 \pm 1.99\%$ in the 5-HT sensitivity assay compared with $54.40 \pm 1.36\%$ for the 14440 control, indicating that serotonin hypersensitivity was restored to normal levels by *epg-8* RNAi. This protective effect was offset by CQ (**Figures 4C, I, J**). Thus, stopping the formation of autophagosomes and reducing their accumulation decreased A β -induced neural damage. 3-MA administration had no additive effects on the basis of *epg-8* RNAi (**Figure 4D**).

The Neuroprotective Effect of Inhibiting Autophagosome Accumulation Requires the Participation of Small Molecular Chaperones

To better understand the A β -induced mechanism of autophagy dysfunction, we performed RNA-seq and proteomic analysis. RNA-seq identified 45 genes that were up-regulated and 111 that were down-regulated in the GMC101 strain compared with the CL2122 control after 8 h A β induction, as well as 881 genes that were up-regulated and 1,034 down-regulated after 24 h induction (**Figures 5A–C**). By enriching the differentially expressed genes associated with autophagy, we identified those with significant differences (**Tables 3, 4**). The results of qPCR supported RNA-seq findings (**Figure 5F** and **Table 1**), and showed that autophagy-related gene expression trends were inconsistent which implies that complex changes occur in the autophagy pathway during A β induction.

Proteomic data showed that 273 proteins were up-regulated and 301 were down-regulated in the GMC101 strain compared with the CL2122 control after A β induction (**Figure 5D**). After using KEGG, we found that autophagy signaling pathways were enriched as differential signaling pathways between CL2122 and GMC101 strains (**Figure 5E**). Among the top 50 up-regulated proteins, we found that let-363 protein (mammalian mTOR) was significantly up-regulated. This also explained why the transcription level of autophagosome formation genes is down-regulated. These results indicated that A β induction impacts on the autophagy signaling pathway and generated a series of downstream events.

To explore the neuroprotective effect of 3-MA, we again conducted RNA-seq (data not shown) and identified 70 KEGG pathways that were enriched with differentially expressed genes between GMC101 and 3-MA groups. Significantly enriched pathways included the Wnt signaling pathway, transforming growth factor-beta signaling pathway, ubiquitin-mediated proteolysis, and protein processing in the endoplasmic reticulum, suggesting that inhibiting autophagosome formation activates pathways that maintain protein homeostasis.

TABLE 2 | Paralysis assay in CL4176 strain nematodes.

	N	PT ₅₀	P-value	Extension percentage (%)
Control	3	3.70 ± 0.10		
10 μM 3-MA	3	4.83 ± 0.20	0.007**	30.54
30 mM CQ	3	2.30 ± 0.06	0.0003***	-37.84
l4440	3	2.46 ± 0.14		
epg-8 RNAi	3	3.10 ± 0.05	0.0155*	26.01
epg-8 RNAi CQ	3	2.06 ± 0.26	ns	-16.26
l4440	3	4.66 ± 0.15		
hsp-16.2 RNAi	3	3.97 ± 0.18	0.0375*	-14.99
hsp-16.2 RNAi 3-MA	3	3.36 ± 0.40	0.0392*	-27.80
l4440	3	4.16 ± 0.03		
hsp-70 RNAi	3	3.56 ± 0.33	0.0002***	-14.00
hsp-70 RNAi 3-MA	3	2.86 ± 0.12	0.0005***	-31.19

The experimental method and the number of repetitions have been stated in the method. * $p < 0.05$; ** $p < 0.01$; *** $p < 0.001$.

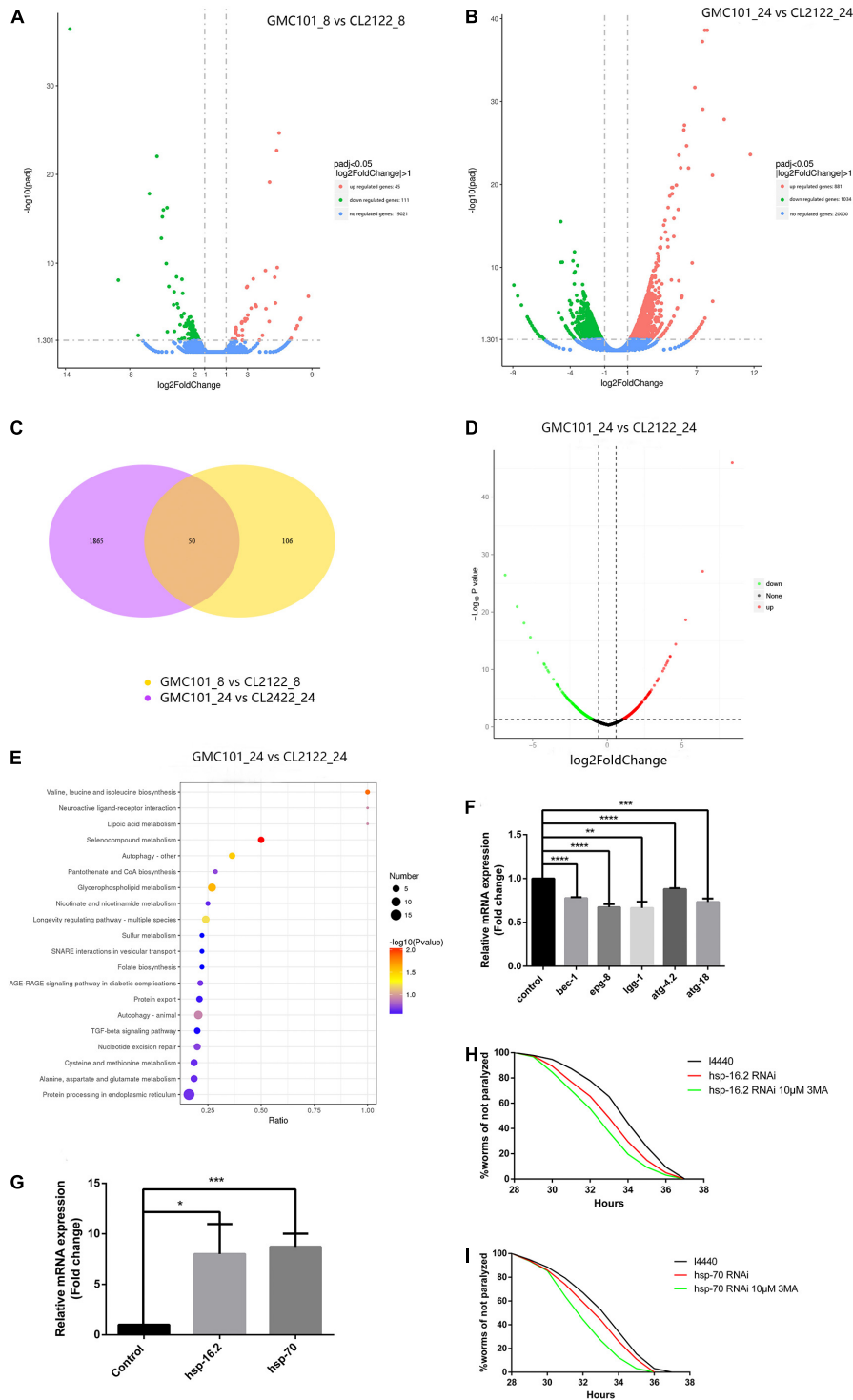


FIGURE 5 | Molecular chaperones are essential for Aβ toxicity in transgenic nematodes. **(A)** After 8 h Aβ induction, 45 genes were up-regulated and 111 down-regulated in GMC101 compared with CL2122 strains. **(B)** After 24 h Aβ induction, 881 genes were up-regulated and 1034 down-regulated in GMC101 compared with CL2122 strains. **(C)** Venn diagram showing the overlap among genes showing significant differential expression ($p < 0.05$) between samples. **(D)** After 24 h Aβ induction, 273 proteins were up-regulated and 301 down-regulated in GMC101 compared with CL2122 strains. **(E)** KEGG pathway enrichment of differentially expressed proteins between CL2122 and GMC101 strains. x and y axes represent GeneRatio and enriched KEGG pathway, respectively. Color represents enrichment significance, and bubble size represents gene count. **(F)** Validation of differentially expressed genes screened by RNA-seq ($n = 3$, $**p < 0.01$; $***p < 0.001$; $****p < 0.0001$ by the Student's t -test). **(G)** Validation of differentially expressed genes screened by RNA-seq. The CL4176 strain was fed either vector I4440 control bacteria or bacteria expressing RNAi for *hsp-16.2* **(H)** and *hsp-70* **(I)**. RNAi for molecular chaperones accelerated Aβ-induced paralysis in the CL4176 strain ($n = 3$, $*p < 0.05$ by the log-rank test).

Autophagy and molecular chaperones were previously shown to have compensatory phenomena in the degradation of misfolded proteins (Park and Cuervo, 2013). Here, we observed a significant increase in the expression of molecular chaperone genes after A β induction by RNA-seq (Tables 3, 4). These findings were verified by qPCR (Figure 5G and Table 1), suggesting that the protective effect of 3-MA requires molecular chaperones. We performed RNAi on the small molecule chaperones *hsp16.2* and *hsp-70* (Figures 5H,I), which reversed the effect of 3-MA in delaying the paralysis time (Table 2). This strongly indicates that the effect of 3-MA in prolonging nematode paralysis depends on the participation of small molecular chaperones.

DISCUSSION

Although AD is the most common neurodegenerative disease, its pathogenesis remains unclear (Lane et al., 2018). Here, we used the *C. elegans* AD model to study autophagy dysfunction as a pathological phenomenon following the transgenic expression of human A β . We verified that protein homeostasis was disrupted and that autophagosome accumulation occurred following the induction of A β expression in *C. elegans* (Figure 1). Autophagosome accumulation in the brain was previously shown to mainly result from reduced lysosomal activity (Sarkis et al., 1988), dynein transport disorders (Lee et al., 2011), and abnormal fusion (Yang et al., 2019).

In our study, we first evaluated the activity of lysosomes regulated by aging (Cairo and Villarroya, 2020) or A β (Song et al., 2020) in AD. However, we found that A β induction enhanced nematode lysosome activity (Figure 2B), which manifested as significant changes in the transcription of V-ATPase and cathepsin genes (Figure 2A and Table 1). V-ATPase is responsible for transferring H⁺ from the cytoplasm to the lysosome (Ernststrom et al., 2012), while cathepsin B and cathepsin D are thought to degrade A β (Hook et al., 2020). The observed enhancement of lysosomal activity and activated cathepsin

transcription suggested that lysosomes are highly sensitive to misfolded proteins under non-aging conditions. However, lysosomal activity is continuously reduced during aging, and the A β degradation ability is also weakened, leading to further aggravation of abnormal autophagy. We used CQ to mimic autophagy deterioration through aging, which confirmed our speculation (Figures 3E–G), and showed that lysosomes are key organelles for maintaining protein homeostasis.

After ruling out lysosome inactivation as causative of autophagosome accumulation, we explored other influencing factors. Dynein transport was also excluded in our nematode model (muscle cells are morphologically different from nerve cells, and lysosomal transport is less dependent on dynein), suggesting that autophagosome accumulation was most likely caused by abnormal lysosome fusion. This was confirmed by our ROS measurements (Figure 2D) and detection of fusion gene transcription (Figure 2E). Both the perforin effect of A β (Julien et al., 2018) and A β -induced oxidative stress can lead to abnormal fusion. However, the exact mechanism is still unclear, and requires further study.

3-MA was reported to have therapeutic effects in cerebral ischemia injury models by reducing autophagosome accumulation (Wang and Wu, 2020). We observed that 10 μ M 3-MA prolonged the paralysis time in the CL4176 strain and had a neuroprotective effect in the A β transgenic nematode model (Figures 3E–G). Reducing autophagosome formation by RNAi had the same effect (Figure 4), suggesting that an imbalance of protein homeostasis caused by abnormal autophagy could be relieved by inhibiting autophagosome formation. On the one hand, reducing the number of abnormal organelles alleviates the stress level, on the other hand it may activate the UPS signaling pathway to improve intracellular pressure. Therefore, maintaining basic levels of autophagy is important in AD treatment.

TABLE 3 | Autophagy-related gene expression after 8 h A β induction.

Wormbase ID	Gene name	Log ₂ (Foldchange)
WBGene00002015	<i>hsp-16.1</i>	10.73201484
WBGene00002019	<i>hsp-16.48</i>	9.993542326
WBGene00002020	<i>hsp-16.49</i>	9.414459887
WBGene00002026	<i>hsp-70</i>	8.695174305
WBGene00002016	<i>hsp-16.2</i>	7.349540251
WBGene00002018	<i>hsp-16.41</i>	7.128486268
WBGene00002017	<i>hsp-16.11</i>	6.349008531
WBGene00002021	<i>hsp-17</i>	1.62722773
WBGene00002008	<i>hsp-4</i>	1.491200843
WBGene00000785	<i>cpr-5</i>	1.427380633
WBGene00002007	<i>hsp-3</i>	1.303493789
WBGene00002011	<i>hsp-12.2</i>	1.280543166
WBGene00006921	<i>vha-12</i>	1.094806355
WBGene00008427	<i>atg-10</i>	-1.583421545

TABLE 4 | Autophagy-related gene expression after 24 h A β induction.

Wormbase ID	Gene name	Log ₂ (Foldchange)
WBGene00002026	<i>hsp-70</i>	3.976840027
WBGene00011906	<i>hsp-12.1</i>	2.032493207
WBGene00006914	<i>vha-5</i>	1.845318311
WBGene00000785	<i>cpr-5</i>	1.266866182
WBGene00021070	<i>cpr-8</i>	1.215308479
WBGene00002023	<i>hsp-25</i>	1.107285903
WBGene00002024	<i>hsp-43</i>	1.111466983
WBGene00006915	<i>vha-6</i>	1.049060101
WBGene00008427	<i>atg-10</i>	-2.831118741
WBGene00002982	<i>lgg-3</i>	-1.63575482
WBGene00014080	<i>atg-4.2</i>	-1.497132712
WBGene00019427	<i>atg-16.2</i>	-1.407504423
WBGene00017178	<i>atg-16.1</i>	-1.272882712
WBGene00018294	<i>atg-18</i>	-1.175782797
WBGene00013695	<i>epg-8</i>	-1.159589162
WBGene00010882	<i>atg-7</i>	-1.124701339
WBGene00002980	<i>lgg-1</i>	-1.092218465
WBGene00021922	<i>atg-3</i>	-1.046291041

Molecular chaperones were previously shown to be up-regulated following A β expression in an AD model (Lackie et al., 2017). Moreover, wild-type A β , but not an A β single chain dimer, could be sequestered in HSP-16.2-containing inclusions (Ai et al., 2018), suggesting the existence of a conformation-dependent interaction between chaperone and A β *in vivo*. We detected significant changes in small molecular chaperone expression at both the transcription and protein levels following A β induction (Table 1). Additionally, the paralysis rate was significantly increased when we used RNAi to decrease heat shock protein gene transcription in the CL4176 strain (Figures 5H,I), indicating that small molecular chaperones play a key role in maintaining protein homeostasis. It is reported that there is a compensatory mechanism between the ways to maintain protein homeostasis (Ji and Kwon, 2017). We hypothesize that 3-MA reduces autophagosome formation and has a protective effect that is molecular chaperone-dependent. RNAi on the small molecule chaperones hsp16.2 and hsp-70 reversed the neuroprotective effect of 3-MA, indicating that it requires the participation of chaperones.

Autophagy is a double-edged sword in AD (Yin et al., 2017), because enhanced autophagy is thought to have therapeutic effects (Friedman et al., 2015), but the accumulation of autophagosomes in the brain can cause serious oxidative stress and trigger apoptosis. Taken together, our findings show that maintaining normal levels of autophagy and lysosomal activity and reducing autophagosome accumulation could relieve A β -induced injuries. Further study is needed to explore the relationship between protein homeostasis and A β , which is essential for the treatment of AD.

DATA AVAILABILITY STATEMENT

The datasets presented in this study can be found in online repositories. The names of the repository/repositories and accession number(s) can be found below: <https://www.ncbi.nlm.nih.gov/geo/>, GSE198684.

REFERENCES

- Ai, L., Yang, F., Song, J., Chen, Y., Xiao, L., Wang, Q., et al. (2018). Inhibition of abeta proteotoxicity by paeoniflorin in *Caenorhabditis elegans* through regulation of oxidative and heat shock stress responses. *Rejuvenation Res.* 21, 304–312. doi: 10.1089/rej.2017.1966
- Cairo, M., and Villarroya, J. (2020). The role of autophagy in brown and beige adipose tissue plasticity. *J. Physiol. Biochem.* 76, 213–226. doi: 10.1007/s13105-019-00708-1
- Chang, J. T., Kumsta, C., Hellman, A. B., Adams, L. M., and Hansen, M. (2017). Spatiotemporal regulation of autophagy during *Caenorhabditis elegans* aging. *eLife* 6:e18459.
- Chen, X. Y., Liao, D. C., Sun, M. L., Cui, X. H., and Wang, H. B. (2020). Essential oil of *Acorus tatarinowii* schott ameliorates abeta-induced toxicity in *Caenorhabditis elegans* through an autophagy pathway. *Oxid. Med. Cell Longev.* 2020:3515609. doi: 10.1155/2020/3515609
- Drake, J., Link, C. D., and Butterfield, D. A. (2003). Oxidative stress precedes fibrillar deposition of Alzheimer's disease amyloid beta-peptide (1-42) in a transgenic *Caenorhabditis elegans* model. *Neurobiol. Aging* 24, 415–420. doi: 10.1016/s0197-4580(02)00225-7

AUTHOR CONTRIBUTIONS

HL, HW, and XC conceived and designed the experiments. HL, YG, and CZ performed the experiments. HL, BM, and MW analyzed the data. HL, HW, and XC wrote the manuscript. All authors read and approved the final manuscript.

FUNDING

This research was funded by the National Natural Science Foundation (grant nos. 31670347, 81001369, and 31170327) and the Shanghai Science and Technology Commission of Shanghai Municipality (grant no. 21015800500).

ACKNOWLEDGMENTS

We thank the CGC Center and J. Fei (Tongji University, Shanghai, China) for providing the worm culture. We thank Malene Hansen for the plasmid of pMH878. We thank Sarah Williams, Ph.D., from Liwen Bianji (Edanz) (www.liwenbianji.cn/) for editing the English text of a draft of this manuscript.

SUPPLEMENTARY MATERIAL

The Supplementary Material for this article can be found online at: <https://www.frontiersin.org/articles/10.3389/fnagi.2022.885145/full#supplementary-material>

Supplementary Table 1 | The 8 h RNA-seq differential gene data.

Supplementary Table 2 | The 24 h differential gene data.

Supplementary Table 3 | The proteomic differential protein data.

Supplementary Data Sheet 1 | The primer list.

- Ernstrom, G. G., Weimer, R., Pawar, D. R., Watanabe, S., Hobson, R. J., Greenstein, D., et al. (2012). ATPase V1 sector is required for corpse clearance and neurotransmission in *Caenorhabditis elegans*. *Genetics* 191, 461–475. doi: 10.1534/genetics.112.139667
- Fabian, T. J., and Johnson, T. E. (1994). Production of age-synchronous mass-cultures of *Caenorhabditis-elegans*. *J. Gerontol.* 49, B145–B156. doi: 10.1093/geronj/49.4.b145
- Florez-McClure, M. L., Hohsfield, L. A., Fonte, G., Bealor, M. T., and Link, C. D. (2007). Decreased insulin-receptor signaling promotes the autophagic degradation of beta-amyloid peptide in *C. elegans*. *Autophagy* 3, 569–580. doi: 10.4161/auto.4776
- Friedman, L. G., Qureshi, Y. H., and Yu, W. H. (2015). Promoting autophagic clearance: viable therapeutic targets in Alzheimer's disease. *Neurotherapeutics* 12, 94–108. doi: 10.1007/s13311-014-0320-z
- Ghosh, D., LeVault, K. R., Barnett, A. J., and Brewer, G. J. (2012). A reversible early oxidized redox state that precedes macromolecular ROS damage in aging nontransgenic and 3xTg-AD mouse neurons. *J. Neurosci.* 32, 5821–5832. doi: 10.1523/JNEUROSCI.6192-11.2012
- Hook, V., Yoon, M., Mosier, C., Ito, G., Podvin, S., Head, B. P., et al. (2020). Cathepsin B in neurodegeneration of Alzheimer's disease, traumatic brain

- injury, and related brain disorders. *Biochim. Biophys. Acta Proteins Proteom.* 1868:140428. doi: 10.1016/j.bbapap.2020.140428
- Huang, Y., and Mucke, L. (2012). Alzheimer mechanisms and therapeutic strategies. *Cell* 148, 1204–1222. doi: 10.1016/j.cell.2012.02.040
- Imanikia, S., Ozbey, N. P., Krueger, C., Casanueva, M. O., and Taylor, R. C. (2019). Neuronal XBP-1 activates intestinal lysosomes to improve proteostasis in *C. elegans*. *Curr. Biol.* 29, 2322.e7–2338.e7. doi: 10.1016/j.cub.2019.06.031
- Ji, C. H., and Kwon, Y. T. (2017). Crosstalk and interplay between the ubiquitin-proteasome system and autophagy. *Mol. Cells* 40, 441–449. doi: 10.14348/molcells.2017.0115
- Julien, C., Tomberlin, C., Roberts, C. M., Akram, A., Stein, G. H., Silverman, M. A., et al. (2018). In vivo induction of membrane damage by beta-amyloid peptide oligomers. *Acta Neuropathol. Commun.* 6:131. doi: 10.1186/s40478-018-0634-x
- Keith, S. A., Maddux, S. K., Zhong, Y. Y., Chinchankar, M. N., Ferguson, A. A., Ghazi, A., et al. (2016). Graded proteasome dysfunction in *Caenorhabditis elegans* activates an adaptive response involving the conserved SKN-1 and ELT-2 transcription factors and the autophagy-lysosome pathway. *PLoS Genet.* 12:e1005823. doi: 10.1371/journal.pgen.1005823
- Lackie, R. E., Maciejewski, A., Ostapchenko, V. G., Marques-Lopes, J., Choy, W. Y., Duennwald, M. L., et al. (2017). The Hsp70/Hsp90 chaperone machinery in neurodegenerative diseases. *Front. Neurosci.* 11:254. doi: 10.3389/fnins.2017.00254
- Lane, C. A., Hardy, J., and Schott, J. M. (2018). Alzheimer's disease. *Eur. J. Neurol.* 25, 59–70.
- Lee, S., Sato, Y., and Nixon, R. A. (2011). Lysosomal proteolysis inhibition selectively disrupts axonal transport of degradative organelles and causes an Alzheimer's-like axonal dystrophy. *J. Neurosci.* 31, 7817–7830. doi: 10.1523/JNEUROSCI.6412-10.2011
- Li, L., Chen, Y., Chenzhao, C., Fu, S., Xu, Q., and Zhao, J. (2018). Glucose negatively affects Nrf2/SKN-1-mediated innate immunity in *C. elegans*. *Aging* 10, 3089–3103. doi: 10.18632/aging.101610
- Li, Q., Liu, Y., and Sun, M. (2017). Autophagy and Alzheimer's disease. *Cell Mol. Neurobiol.* 37, 377–388.
- Lipinski, M. M., Zheng, B., Lu, T., Yan, Z., Py, B. F., Ng, A., et al. (2010). Genome-wide analysis reveals mechanisms modulating autophagy in normal brain aging and in Alzheimer's disease. *Proc. Natl. Acad. Sci. U.S.A.* 107, 14164–14169. doi: 10.1073/pnas.1009485107
- Mangialasche, F., Solomon, A., Winblad, B., Mecocci, P., and Kivipelto, M. (2010). Alzheimer's disease: clinical trials and drug development. *Lancet Neurol.* 9, 702–716.
- Martin, E., Boucher, C., Fontaine, B., and Delarasse, C. (2017). Distinct inflammatory phenotypes of microglia and monocyte-derived macrophages in Alzheimer's disease models: effects of aging and amyloid pathology. *Aging Cell.* 16, 27–38. doi: 10.1111/acel.12522
- Palmisano, N. J., Rosario, N., Wysocki, M., Hong, M., Grant, B., and Melendez, A. (2017). The recycling endosome protein RAB-10 promotes autophagic flux and localization of the transmembrane protein ATG-9. *Autophagy* 13, 1742–1753. doi: 10.1080/15548627.2017.1356976
- Park, C., and Cuervo, A. M. (2013). Selective autophagy: talking with the UPS. *Cell Biochem. Biophys.* 67, 3–13. doi: 10.1007/s12013-013-9623-7
- Sangha, J. S., Wally, O., Banskota, A. H., Stefanova, R., Hafting, J. T., Critchley, A. T., et al. (2015). A cultivated form of a red seaweed (*Chondrus crispus*), suppresses beta-amyloid-induced paralysis in *Caenorhabditis elegans*. *Mar. Drugs* 13, 6407–6424. doi: 10.3390/md13106407
- Sarkis, G. J., Ashcom, J. D., Hawdon, J. M., and Jacobson, L. A. (1988). Decline in protease activities with age in the nematode *Caenorhabditis elegans*. *Mech. Ageing Dev.* 45, 191–201. doi: 10.1016/0047-6374(88)90001-2
- Savelieff, M. G., Nam, G., Kang, J., Lee, H. J., Lee, M., and Lim, M. H. (2019). Development of multifunctional molecules as potential therapeutic candidates for Alzheimer's disease, parkinson's disease, and amyotrophic lateral sclerosis in the last decade. *Chem. Rev.* 119, 1221–1322. doi: 10.1021/acs.chemrev.8b00138
- Selkoe, D. J., and Hardy, J. (2016). The amyloid hypothesis of Alzheimer's disease at 25 years. *EMBO Mol. Med.* 8, 595–608. doi: 10.15252/emmm.201606210
- Song, L., Yao, L., Zhang, L., Piao, Z., and Lu, Y. (2020). Schizandrol A protects against A β 1-42-induced autophagy via activation of PI3K/AKT/mTOR pathway in SH-SY5Y cells and primary hippocampal neurons. *Naunyn-Schmiedeberg's Arch. Pharmacol.* 393, 1739–1752. doi: 10.1007/s00210-019-01792-2
- Sorrentino, V., Romani, M., Mouchiroud, L., Beck, J. S., Zhang, H., D'Amico, D., et al. (2017). Enhancing mitochondrial proteostasis reduces amyloid-beta proteotoxicity. *Nature* 552, 187–193. doi: 10.1038/nature25143
- Springhorn, A., and Hoppe, T. (2019). Western blot analysis of the autophagosomal membrane protein LGG-1/LC3 in *Caenorhabditis elegans*. *Methods Enzymol.* 619, 319–336. doi: 10.1016/bs.mie.2018.12.034
- Wang, X., Sun, D., Hu, Y., Xu, X., Jiang, W., Shang, H., et al. (2019). The roles of oxidative stress and Beclin-1 in the autophagosome clearance impairment triggered by cardiac arrest. *Free Radic. Biol. Med.* 136, 87–95. doi: 10.1016/j.freeradbiomed.2018.12.039
- Wang, X., and Wu, Y. (2020). Protective effects of autophagy inhibitor 3-methyladenine on ischemia-reperfusion-induced retinal injury. *Int. Ophthalmol.* 40, 1095–1101. doi: 10.1007/s10792-019-01272-9
- Wu, Y., Wu, Z., Butko, P., Christen, Y., Lambert, M. P., Klein, W. L., et al. (2006). Amyloid-beta-induced pathological behaviors are suppressed by Ginkgo biloba extract EGb 761 and ginkgolides in transgenic *Caenorhabditis elegans*. *J. Neurosci.* 26, 13102–13113. doi: 10.1523/JNEUROSCI.3448-06.2006
- Yang, H., Shen, H., Li, J., and Guo, L. W. (2019). SIGMAR1/Sigma-1 receptor ablation impairs autophagosome clearance. *Autophagy* 15, 1539–1557. doi: 10.1080/15548627.2019.1586248
- Yang, Z. Z., Yu, Y. T., Lin, H. R., Liao, D. C., Cui, X. H., and Wang, H. B. (2018). *Lonicera japonica* extends lifespan and healthspan in *Caenorhabditis elegans*. *Free Radic. Biol. Med.* 129, 310–322. doi: 10.1016/j.freeradbiomed.2018.09.035
- Yin, Y., Sun, G., Li, E., Kiselyov, K., and Sun, D. (2017). ER stress and impaired autophagy flux in neuronal degeneration and brain injury. *Ageing Res. Rev.* 34, 3–14. doi: 10.1016/j.arr.2016.08.008
- Yu, G., Wang, L. G., Han, Y., and He, Q. Y. (2012). clusterProfiler: an R package for comparing biological themes among gene clusters. *OMICS* 16, 284–287. doi: 10.1089/omi.2011.0118
- Zare-Shahabadi, A., Masliah, E., Johnson, G. V., and Rezaei, N. (2015). Autophagy in Alzheimer's disease. *Rev. Neurosci.* 26, 385–395.
- Zeng, M., and Zhou, J. N. (2008). Roles of autophagy and mTOR signaling in neuronal differentiation of mouse neuroblastoma cells. *Cell Signal.* 20, 659–665. doi: 10.1016/j.cellsig.2007.11.015
- Zhang, H., and Baehrecke, E. H. (2015). Eaten alive: novel insights into autophagy from multicellular model systems. *Trends Cell Biol.* 25, 376–387. doi: 10.1016/j.tcb.2015.03.001
- Zhang, X. G., Wang, X., Zhou, T. T., Wu, X. F., Peng, Y., Zhang, W. Q., et al. (2016). Scorpion venom heat-resistant peptide protects transgenic *Caenorhabditis elegans* from beta-amyloid toxicity. *Front. Pharmacol.* 7:227. doi: 10.3389/fphar.2016.00227
- Zhu, Z., Yang, T., Zhang, L., Liu, L., Yin, E., Zhang, C., et al. (2019). Inhibiting A β toxicity in Alzheimer's disease by a pyridine amine derivative. *Eur. J. Med. Chem.* 168, 330–339. doi: 10.1016/j.ejmech.2019.02.052

Conflict of Interest: The authors declare that the research was conducted in the absence of any commercial or financial relationships that could be construed as a potential conflict of interest.

Publisher's Note: All claims expressed in this article are solely those of the authors and do not necessarily represent those of their affiliated organizations, or those of the publisher, the editors and the reviewers. Any product that may be evaluated in this article, or claim that may be made by its manufacturer, is not guaranteed or endorsed by the publisher.

Copyright © 2022 Lin, Gao, Zhang, Ma, Wu, Cui and Wang. This is an open-access article distributed under the terms of the Creative Commons Attribution License (CC BY). The use, distribution or reproduction in other forums is permitted, provided the original author(s) and the copyright owner(s) are credited and that the original publication in this journal is cited, in accordance with accepted academic practice. No use, distribution or reproduction is permitted which does not comply with these terms.